Hysteretic Multiscale formulation for Validating Computational Models of Heterogeneous Structures

Savvas P. Triantafyllou[1] and Eleni N. Chatzi[2]

Abstract

A framework for the development of accurate yet computationally efficient numerical models is proposed in this work, within the context of computational model validation. The accelerated computation achieved herein relies on the implementation of a recently derived multiscale finite element formulation, able to alternate between scales of different complexity. In such a scheme, the fine scale is modeled using a hysteretic finite elements formulation. In the micro-level non-linearity is captured via a set of additional hysteretic degrees of freedom compactly described by an appropriate hysteric law, which gravely simplifies the dynamic analysis task. The computational efficiency of the scheme is rooted in the interaction between the micro- and a macro-mesh level, defined through suitable interpolation fields that map the finer mesh displacement field to the coarser mesh displacement field. Furthermore, damage related phenomena that are manifested at the micro-level are accounted for using a set of additional evolution equations corresponding to the stiffness degradation and strength deterioration of the underlying material. The developed modeling approach is utilized for the purposes of model validation; firstly, in the context of reliability analysis; and secondly, within an inverse problem where the identification of constitutive parameters via availability of acceleration response data is sought.

Introduction

Engineering simulation is an essential feature accompanying the design, manufacturing and operational life of every engineered structure. However, and despite the refinement and complexity that such simulations might entail, these are not routinely validated, largely due to the computational cost associated with the multiplicity of parallel runs involved. This inadequacy comes in direct disagreement with the recent advances both in monitoring methodologies as well as in computation potential. The former has provided engineers with low-cost means of assessing structural performance both during the construction phase as well as during the operational of a structural system. Significant feedback is therefore collected from the system at hand, which may then be utilized for selecting, updating and/or validating candidate computational models.

A significant source of complexity within computation stems from the potential multi-phase nature of materials comprising the system to be analyzed. Multiphase materials, also known as composites, fit the profile of emerging material solutions calling for enhanced computation. In most industrial cases, the main volume of a composite consists of a single material (e.g. the matrix) that acts as a basis where a number of reinforcing materials are added. The distribution of the reinforcement within the matrix can be either fully prescribed (as in the case of layered composites) or random (as in the case of fiber reinforced matrices). This process of mechanically combining constituent materials baring different properties results into a highly heterogeneous structure. Due to the advanced material properties of the resulting medium

(e.g. high stiffness to weight ratios, high damping, negative Poisson's ratio and high toughness (Strong 2008)) composites are widely used in numerous applications. Moreover, research efforts are oriented towards further improving the mechanical properties of composites while at the same time alleviating some of their disadvantages such as high production/ implementation costs and damage susceptibility (Rohatgi 1994; Saheb and Jog 1999; Peng et al. 2011). Recent advances in fields such as bioengineering, nano-mechanics and electronics also stress the need for designing new composites with optimum material properties (Munch et al. 2008; Belingardi et al. 2013). Nonetheless, prior to proceeding with design refinement, methodologies for validating the efficacy of the numerical models simulating these solutions need to be developed.

Model validation may be carried out via two distinct routes, which however can be intertwined. The first path is though numerical validation, in the sense that the final model to be utilized is usually inferred by adoption of a number of assumptions which simplify the analysis thereby reducing the required computational toll. A first step for validating such models is through comparison with more refined/higher dimensional numerical solutions that avoid

[1] Department of Civil Engineering, The University of Nottingham, UK
[2] Institute of Structural Engineering, Department of Civil, Environmental and Geomatic Engineering, ETH Zürich, Switzerland

Corresponding author:
Eleni Chatzi, Institute of Structural Engineering ETH Zrich, HIL E 14.3, Stefano-Franscini-Platz 5, CH-8093 Zrich, Switzerland.
Email: chatzi@ibk.baug.ethz.ch

a large number of assumptions at the cost, however, of an exhaustive computation. If the reduced order model successfully reproduces the desired response with a sufficient level of accuracy, lying within some acceptable threshold, it may then be adopted for the forward simulation of the system at hand. The second route, which is invaluable within the context of standardization of the validation approach, is through experimental validation as noted in the work of Patterson et al. (2012); Felipe-Sesé et al. (2014); Burguete et al. (2013). This route relies on the use of actual structural feedback, i.e., through experimental or field measurements of structural response under static or dynamic loads. Indeed, when it comes to composites, significant effort has been allocated in developing simulation models that comply with experimentally measured response, via an inverse problem formulation (Soares et al. 1993). In past years, several methods have been introduced along the lines of the so-called mixed numerical-experimental techniques for the successful modeling of polymer based materials and composite reinforcing textiles (Frederiksen 1997; Rikards et al. 1999). The anisotropic and heterogeneous nature of these materials turns the direct determination of stiffness parameters into an arduous task. Conventional methods are based on direct measurements of strain fields (Tucker and Erwin 1999), presenting several drawbacks such as boundary effects, sample size dependencies and difficulties in obtaining homogeneous stress/strain fields (Aboudi 2013). As an alternative, indirect methods based on modal test data have become more popular in recent years. These are based on measurements of structural response and the comparison between the experimentally identified eigen-frequencies of a structure and those obtained through a numerical analysis employing a finite element model (Maletta and Pagnotta 2004; Ekel'chik 2007; Abrosimov and Kulikova 2011). This inverse problem formulation can lead to an estimate of the macroscopic material parameters of the composite materials, which are generally impossible to standardize in tables or databases as they are dependent on diverse factors such as the geometrical arrangement of the laminates, constituent materials used, manufacturing process etc. Independent of whether a direct or indirect method is employed, a forward model of the structure is required for deriving those parameters that are deemed as uncertain, most commonly those pertaining to the effective moduli.

However, the dependence of the identified parameters on the size of the specimen (Bažant and Daniel 1996; Liu et al. 1998) imposes a strong constraint on the required size of the underlying finite element model leading to computationally intensive problems (Pickett 2002). To reduce the computational cost, multiscale simulation approaches have been introduced (Hansun 2009; Pahlavanpour et al. 2013; Nguyen et al. 2012). In general, multiscale methods can be separated in two groups, namely multiscale homogenization methods and multiscale finite element methods (MsFEMs). Within the framework of the averaging theory for ordinary and partial differential equations, multiscale homogenization methods are based on the evaluation of an averaged strain and corresponding stress tensor over a predefined space domain denoted as Representative Volume (RVE) (Babuška 1975). Amongst the various homogenization methods proposed (Geers et al.

2010), the asymptotic homogenization method is proven to be efficient in terms of accuracy and required computational cost (Yu and Fish 2002). An extensive review on the subject can be found in (Kanouté et al. 2009).

Although homogenization methods are based on a strong and robust mathematical background, they rely on the assumption of scale separation and local periodicity of the underlying micro-structure. Many structures however usually fail to adhere to these assumptions, due to the non-periodic nature of the imposed boundary and loading conditions that lead to non-periodic stress and strain fields as well as the non-deterministic distribution of heterogeneities within them. To overcome this deficiencies the multiscale finite element method has been introduced, which relies on the numerical evaluation of a set of micro-scale basis functions that are used to map the micro-structure information onto the larger scale. MsFEMs have been extensively used in linear and nonlinear flow simulation analysis (Efendiev et al. 2005; He and Ren 2005). Recently, the Enhanced Multiscale Finite Element method (EMsFEM) has been proposed for the linear and nonlinear static analysis of heterogeneous structures (Zhang et al. 2012). EMsFEM introduces additional coupling terms into the fine-scale interpolation functions to consider the coupling effect among different directions in multi-dimensional vector problems. However, the evaluation of the micro-scale basis functions is based on the solution of a boundary value problem rendering the interpolation scheme material dependent. Consequently, this numerical mapping needs to be evaluated in every step of a non-linear incremental analysis procedure, thus alleviating the computational advantages of the method.

Dynamic forces and repeated cyclic loading beyond a material's elastic limit often lead to damage accumulation and therefore to nonlinear response, which further complicates the implementation of the aforementioned EMsFEM framework. Damage initiates at the micro-level through the propagation of inherent micro-discontinuities and manifests itself at the meso- and macro-scale finally resulting in the gradual reduction of the strength and stiffness of the structure which is observed at the macro-scale. Within this framework, the hysteretic multiscale finite element method (HMsFEM) has been introduced in recent work of the authors Triantafyllou and Chatzi (2014), for the efficient treatment of nonlinear dynamic analysis of heterogeneous structures. In this, the fine mesh is modelled using the hysteretic formulation of finite elements (Triantafyllou and Koumousis 2014), which is based on the definition of a set of additional degrees of freedom that account for the evolution of the plastic part of the deformation component within the element. Since inelasticity is treated as a degree of freedom, the stiffness matrix of the element remains constant throughout the analysis procedure. As a result, the evaluation of the of the micro-basis functions is also performed once. The evolution of the additional degrees of freedom is constrained by a set of additional equations that account for the constitutive behavior of the underlying material. A smooth plasticity model is used to account for the evolution of plastic strains at the micro-scale. In this work, damage accumulation is also accounted for by introducing a set of internal variables accounting for damage the gradual degradation of the material's unloading stiffness as well as the deterioration of the material's yield limit.

In the work presented herein, the previously introduced HMsFEM approach serves as the tool for model validation, under a stochastic setting in two classes of problems. The first application pertains to a reliability analysis problem, where the structural response is quantified in a probabilistic sense using a Monte Carlo approach. Since the nature of composite materials comes with significant uncertainties as to the properties of the individual constituents (Xu et al. 2011; Clément et al. 2013), the stochastic analysis of such materials under conditions of extreme loading is of paramount importance in order to quantify the probability of failure of the corresponding structure. Since the reliability analysis of structures per-se is a computationally intense procedure, it is pointed out that multiscale models (Tootkaboni and Graham-Brady 2010) should be preferred over standard stochastic FEM procedures (Shang and Yun 2013) to reduce the complexity of the implemented computational model without adverse effects on the desired accuracy. The second application pertains to an inverse problem formulation, where the identification of the uncertain material parameters of a composite structure, namely the structural stiffness and strength at the level of the constituents, is sought, based on recorded acceleration response from limited structural nodes.

The paper is structured as follows. In Section **The enhanced multiscale finite element method** the Enhanced Multiscale Finite Element Method (EMsFEM) is overviewed. The smooth hysteretic model that forms the basis of the proposed method is described in Section **Hysteretic modeling in the fine scale**. In Section **The hysteretic multiscale finite element method** the Hysteretic Multiscale Finite Element Method (HMsFEM) is presented. Section **Computational Model Validation** briefly discusses the computational tools that are here adopted for the purpose of model validation, from both a numerical and experimental standpoint. Finally, examples are presented in Section **Examples** to validate the proposed derivations and demonstrate the computational advantages of the developed framework, firstly under the scope of reliability assessment and secondly within the context of an inverse problem formulation. The adoption of enhanced and cost-effective simulation approaches in the validation process can grease the wheels of the process chain from design, through manufacturing and production, to operation and maintenance.

The enhanced multiscale finite element method

Overview

EMsFEM is based on the definition of a set of nested finite element meshes as explained in Zhang et al. (2012). The interaction between subsequent mesh levels is defined through the numerical derivation of corresponding interpolation fields that map the finer mesh displacement field to the coarser mesh displacement field. In Fig. 1(a), the case of a two-phase solid composite structure is presented for brevity. The composite comprises a matrix and a set of reinforcing cells. Based on the distribution of the cells within the matrix, a fine discretization scheme is defined, consisting

of 384 linear hex-elements and 663 nodes that correspond to 1989 degrees of freedom.

Depending on the micro-structure's periodicity, patterns of heterogeneity can be recognized and sets of micro-elements can be grouped into clusters (that will be denoted herein as Representative Volume Elements or RVEs). The convex-hull of each cluster defines a coarse-element (or macro-element) that surrounds the fine-meshed RVE substructure. In Fig.1 two distinct patterns are identified and the corresponding RVEs are presented in Fig. 1(c) and 1(d). The set of coarse elements results in the definition of the coarse mesh presented in Fig. 1(e). This mesh consists of 8 coarse elements and 30 macro-nodes that correspond to 90 macro-degrees of freedom.

According to EMsFEM, instead of performing a finite element analysis on the fine mesh (Fig. 1(a)) a numerical interpolation scheme $\mathscr{T}_i$ is evaluated for each RVE (i) that maps the displacements of the corresponding micro-nodes defined within the micro-domain Ω_m onto the macro-displacement field defined in the macro-domain Ω_M. Furthermore, two displacements fields are established corresponding to each level of discretization. Thus, in the fine mesh the displacement of a micro point p is described by the micro-displacement vector field (Fig. 1(h)).

$$\mathbf{u_m} = \left\{ u_m \; v_m \; w_m \right\}^T \big|_{(x,y,z)} \qquad (1)$$

The continuous micro-displacement field introduced in relation (1) can be interpolated at the micro-nodal points using a standard displacement based FE interpolation scheme as in Zienkiewicz et al. (2005)

$$\mathbf{u_m} = [N]_m d_m^i \qquad (2)$$

where

$$d_m^i = \underbrace{\left\{ \; u_{m(1)} \quad v_{m(1)} \quad \cdots \quad v_{m(8)} \; \right\}}_{1x24}^T \qquad (3)$$

is the vector of nodal displacements of the i_{th} micro-element and $[N]_m$ is the displacement based interpolation matrix of the hex-element.

Since the structure defined in Fig. 1(e) is a discrete macro-representation of the physical model consisting of the RVEs, the macro-displacement component within each RVE d_M^i can be defined accordingly as the discrete set such that

$$d_M^i = \underbrace{\left\{ \; u_{M(1)} \quad v_{M(1)} \quad \cdots \quad v_{m(8)} \; \right\}}_{1x24}^T \qquad (4)$$

where (i) stands for the i_{th} macro-node of the coarse mesh.

Throughout this work the subscript m is used to denote a micro-measure while the capital M is used to denote a macro-measure of the indexed quantity. The enhanced multiscale Finite Element method is based on the numerical derivation of a relation between the discrete micro-displacement field introduced in equation (3) and the coarse element discrete displacement field introduced in relation (4).

Numerical evaluation of micro-scale basis functions

The numerical mapping is established by considering each type of coarse element and the corresponding fine mesh
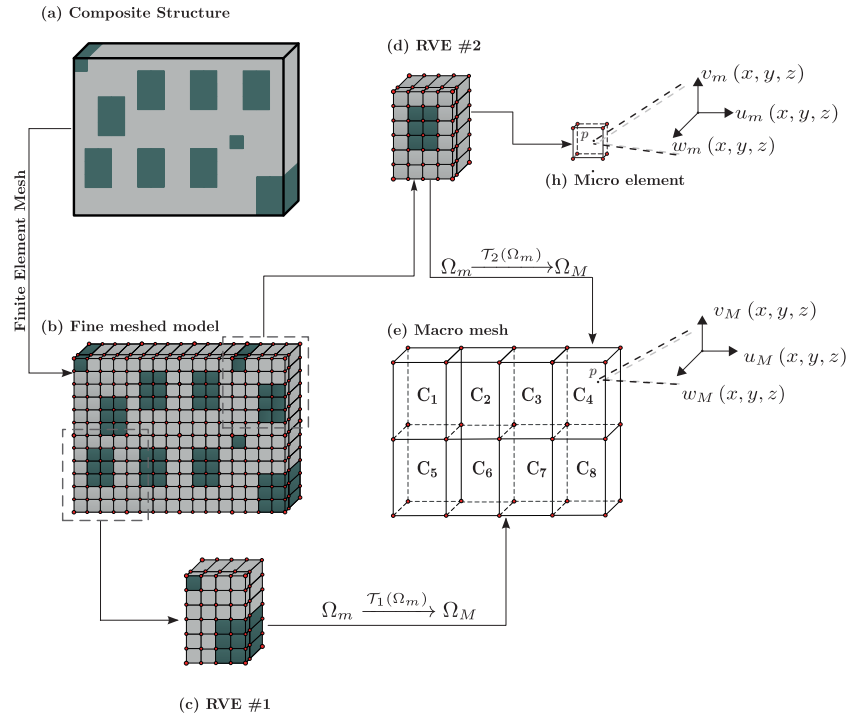
(a) Composite Structure

(d) RVE #2

$v_m(x,y,z)$
$u_m(x,y,z)$
$w_m(x,y,z)$

(h) Micro element

$\Omega_m \xrightarrow{\mathcal{T}_2(\Omega_m)} \Omega_M$

(b) Fine meshed model

(e) Macro mesh

$v_M(x,y,z)$
$u_M(x,y,z)$
$w_M(x,y,z)$

C_1 C_2 C_3 C_4
C_5 C_6 C_7 C_8

$\Omega_m \xrightarrow{\mathcal{T}_1(\Omega_m)} \Omega_M$

(c) RVE #1

Figure 1. Multiscale Finite Element procedure.

within this element as a representative volume element (RVE). For each RVE a homogeneous equilibrium equation is established considering specific boundary conditions. The solution of this equilibrium problem forms a vector of base functions that maps the displacement components of the fine mesh within the element to the macro-nodes of the RVE. EMsFEM is based on the assumption that the discrete micro-displacements within the coarse element are interpolated at the macro-nodes using the following scheme:

$$u_{m(j)} = \sum_{i=1}^{n_{Macro}} N_{ijxx} u_{M_i} + \sum_{i=1}^{n_{Macro}} N_{ijxy} v_{M_i}$$
$$+ \sum_{i=1}^{n_{Macro}} N_{ijxz} w_{M_i}$$
$$v_{m(j)} = \sum_{i=1}^{n_{Macro}} N_{ijxy} u_{M_i} + \sum_{i=1}^{n_{Macro}} N_{ijyy} v_{M_i}$$
$$+ \sum_{i=1}^{n_{Macro}} N_{ijyz} w_{M_i} \quad (5)$$
$$w_{m(j)} = \sum_{i=1}^{n_{Macro}} N_{ijxz} u_{M_i} + \sum_{i=1}^{n_{Macro}} N_{ijyz} v_{M_i}$$
$$+ \sum_{i=1}^{n_{Macro}} N_{ijzz} w_{M_i}$$

where $u_{m(j)}$, $v_{m(j)}$, $w_{m(j)}$ are the displacement components of the j_{th} micro-node, $j = 1...n_{micro}$ where n_{micro} the number of micro nodes within the coarse element. Furthermore, n_{Macro} is the number of macro-nodes of the coarse element and u_{M_i}, v_{M_i}, w_{M_i} are the displacement components of the macro-nodes of the i_{th} coarse-element.

The quantities N_{ijxx}, N_{ijxy}, N_{ijyy}, N_{ijzz}, N_{ijxz}. N_{ijyz} are the micro-basis interpolation functions that interpolate the displacement components of the j_{th} micro-node to the macro-displacement components of the corresponding $i_t h$ coarse element. In MsFEM the interpolated displacement fields are considered uncoupled. However in EMsFEM the coupling terms N_{ijxy}, N_{ijyz}, N_{ijxz} are introduced that are more consistent with the observation that a unit

displacement in the boundary of a deformable body may induce displacements in both directions within the body.

Equation (5) can be conveniently cast in the following matrix form:

$$\{d\}_{m(i)} = [N]_{m(i)} \{d\}_M \quad (6)$$

where $\{d\}_{m(i)}$ is the nodal displacement vector of the i_{th} microelement, $[N]_{m(i)}$ is a matrix containing the micro-basis shape functions evaluated at the nodes of the i_{th} micro-element while $\{d\}_M$ is the vector of nodal displacements of the corresponding macro-nodes. Denoting $\{d\}_m$ the $(3n_{micro} \times 1)$ vector of nodal displacements of the micro-mesh, the following relation is established:

$$\{d\}_m = [N]_m \{d\}_M \quad (7)$$

where $[N]_m$ in equation (7) is a 315×24 matrix containing the components of the micro-basis shape functions evaluated at the nodal points (x_j, y_j, z_j) of the micro-mesh. Each column of matrix $[N]_m$ corresponds to a deformed configuration of the RVE where the corresponding macro-degree of freedom is equal to unity and all the rest macro-degrees of freedom are equal to zero.

Deriving micro-basis functions with these properties can be accomplished by considering the following boundary value problem

$$[K]_{RVE} \{d\}_m = \{\emptyset\}$$
$$\{d\}_S = \{\bar{d}\} \quad (8)$$

where $[K]_{RVE}$ is the stiffness matrix of the RVE, $\{\emptyset\}$ is a vector containing zeros while $\{d\}_S$ is a vector containing the nodal degrees of freedom of the boundary S of the RVE and $\{\bar{d}\}$ is a vector of prescribed displacements. The RVE stiffness matrix is formulated using the standard finite

element method (Zienkiewicz et al. 2005). In this work, the solution of the boundary value problem established in equation (8) is performed using the Penalty method (Maury 2008).

The choice of the values of the prescribed boundary displacements is an assumption of the EMsFEM and plays a key part on the accuracy of the macro-scale solution. Three different types of boundary conditions are established in the literature namely linear boundary conditions, periodic boundary conditions and oscillatory boundary conditions with oversampling. In the first case, the displacements along the boundaries of the coarse element are considered to vary linearly. Periodic boundary conditions are established by considering that the displacement components of periodic nodes lying on the boundary of the coarse element differ by a fixed quantity that varies linearly along the boundary of the coarse element. The oscillatory boundary condition method with oversampling considers a superelement of the coarse element whose basis functions are evaluated using the linear boundary condition approach. The derived basis functions are then used as the boundary conditions of the coarse element to derive the micro basis functions. An illustrative presentation on the subject can be found in Efendiev and Hou (2009).

Hysteretic modeling in the fine scale

Material Model

The hysteretic formulation of finite elements (Triantafyllou and Koumousis 2014) is implemented herein to account for the nonlinear dynamic behavior of materials at the micro-scale. In this, a mixed interpolation scheme is considered for both the displacement and the plastic component of the strain tensor. The method is based on the additive decomposition of the strain rates into a reversible elastic and an irreversible inelastic component (Nemat-Naser 1982) that is defined through the following relation:

$$\{\dot{\varepsilon}\}_{m(i)} = \{\dot{\varepsilon}^{el}\}_{m(i)} + \{\dot{\varepsilon}^{pl}\}_{m(i)} \qquad (9)$$

where $\{\varepsilon\}_{m(i)}$ is the tensor of total strain, $\{\varepsilon^{el}\}_{m(i)}$ is the tensor of the elastic, reversible, strain and $\{\varepsilon^{pl}\}_{m(i)}$ is the tensor of the plastic strain while $m(i)$ indexes the i_{th} micro-element within the coarse element. The vectorial notation of the stress and strain tensors is used in this work while the (.) symbol denotes differentiation with respect to time. In classical elasto-plasticity, the elastic component of the strain tensor $\{\varepsilon^{el}\}_{m(i)}$ is directly related to the current stress $\{\sigma\}_{m(i)}$ through the Hooke's law

$$\{\dot{\sigma}\}_{m(i)} = [D]_{m(i)} \{\dot{\varepsilon}^{el}\}_{m(i)} \qquad (10)$$

where $[D]_{m(i)}$ is the elastic material constitutive matrix (Armenakas 2006). Additionally, an evolution law is considered for the plastic part of the deformation component that can be generically defined as:

$$\{\dot{\varepsilon}^{pl}\}_{m(i)} = \mathscr{F}\left(\{\varepsilon^{el}\}_{m(i)}, \{\dot{\varepsilon}^{el}\}_{m(i)}, \{\sigma\}_{m(i)}\right) \qquad (11)$$

where $\mathscr{F}$ is an hysteretic operator (Visintin 1994; Iwan 1967; Erlicher 2003).

In this work, the hysteretic operator is defined on the grounds of a multi-axial smooth plasticity model (Triantafyllou and Koumousis 2014) based on the assumptions of rate-independent associative plasticity (Lubliner 2008). Within this framework, the evolution of the plastic strain tensor is defined as

$$\{\dot{\varepsilon}^{pl}\}_{m(i)} = H_1 H_2 [R] \{\dot{\varepsilon}\}_{m(i)} \qquad (12)$$

where H_1 and H_2 are smoothened Heaviside functions defined by the following relations, namely:

$$H_1 = \left| \frac{\Phi\left(\{\sigma\}_{m(i)}, \{\eta\}_{m(i)}\right)}{\Phi_0} \right|^N, \quad N \geq 2 \qquad (13)$$

and

$$H_2 = \beta + \gamma sgn\left(\dot{\Phi}\right) \qquad (14)$$

In equation (13) $\Phi = \Phi\left(\{\sigma\}_{m(i)}, \{\eta\}_{m(i)}\right)$ is a yield criterion, Φ_0 the yield limit, N a material parameter that determines the rate at which the yield criterion reaches its maximum value while β and γ are material parameters that control the stiffness at the moment of unloading. The time derivative of the yield function in equation (14) is derived from the following expression

$$\dot{\Phi} = \frac{\partial \Phi}{\partial \{\sigma\}_{m(i)}} \{\dot{\sigma}\}_{m(i)} + \frac{\partial \Phi}{\partial \{\eta\}_{m(i)}} \{\dot{\eta}\}_{m(i)} \qquad (15)$$

Matrix $[R]$ in equation (12) is a strain interaction matrix defined through the following relation

$$[R] = \{\alpha\} Q \{\alpha\}^T [D] \qquad (16)$$

where

$$Q = \left(-\{b\}^T G\left(\{\eta\}_{m(i)}, \Phi\right) + (\alpha)^T [D] \{\alpha\}\right)^{-1} \qquad (17)$$

and column vectors $\{\alpha\}$ and $\{b\}$ are defined as

$$\{\alpha\} = \partial \Phi \big/ \partial \{\sigma\}$$

and

$$\{b\} = \partial \Phi \big/ \partial \{\eta\}$$

respectively, while $G\left(\{\eta\}_{m(i)}, \Phi\right)$ is a hardening function corresponding to the kinematic hardening rule considered and is defined through the following relation

$$\{\dot{\eta}\}_{m(i)} = \lambda G\left(\Phi, \{\eta\}_{m(i)}\right) \qquad (18)$$

where $\dot{\lambda}$

$$\dot{\lambda} = \{\dot{\varepsilon}^{pl}\}_{m(i)} \frac{\partial \Phi}{\partial \{\sigma\}_{m(i)}}$$

is the plastic multiplier of classical plasticity (Lubliner 2008).

Since the yield function in relation (13) depends on the back-stress a second equation is also introduced for the evolution of the back-stress with respect to the strain field that assumes the following form:

$$\{\dot{\eta}\} = H_1 H_2 G\left(\{\eta\}_{m(i)}, \Phi\right) [\tilde{R}] \{\dot{\varepsilon}\}_{m(i)} \qquad (19)$$

where $\left[\tilde{R}\right]$ is the corresponding hardening interaction matrix defined by the following relation

$$\left[\tilde{R}\right] = Q\left\{\alpha\right\}^T [D] \qquad (20)$$

Equations (9) and (10) imply that during unloading the material stiffness is constant and equal to the elastic one.

Cyclic loading induced damage

The model presented in Section **Material Model** is extended herein to account for damage induced deformations. This is accomplished by introducing two additional internal parameters within the hysteretic finite element scheme accounting for the degradation of the elastic material stiffness and the deterioration of the yield limit. These parameters are accompanied by a set of corresponding evolution equations that depend on the hysteretic energy accumulated over time. The relations are based on the derivations introduced in (Erlicher and Point 2004) where a proof is also derived for the thermodynamic admissibility of the corresponding material model.

The elastic stiffness degradation parameter is introduced at the stress-strain relation (10), which assumes the following form

$$\{\dot{\sigma}\}_{m(i)} = v_\eta [D]_{m(i)} \left\{\dot{\varepsilon}^{el}\right\}_{m(i)} \qquad (21)$$

where v_η is a degradation parameter that is equal to unity as long as the material has not yielded and increases as a function of the plastic deformation. The following generic expression is thus defined:

$$\dot{v_\eta} = \mathscr{K}_\eta\left(E_{hm(i)}\right) \qquad (22)$$

where $E_{hm(i)}$ is the hysteretic energy of the i_{th} micro-element.

Solving equation (9) for $\left\{\dot{\varepsilon}^{el}\right\}$ and substituting into equation (21) the following relation is finally derived:

$$\{\dot{\sigma}\}_{m(i)} = v_\eta [D]_{m(i)} \left(\{\dot{\varepsilon}\}_{m(i)} - \left\{\dot{\varepsilon}^{pl}\right\}_{m(i)}\right) \qquad (23)$$

where the total stress tensor is expressed as a function of the total and plastic strain tensors and the degradation parameter. For the purpose of this work, a constant rate stiffness degradation rule is considered and thus relation (22) is expressed as

$$\left.\begin{array}{r} \dot{c_\eta} = \eta_{sd} \\ c_\eta|_{E_h=0} = 1.0 \end{array}\right\} \Rightarrow v_\eta = 1.0 + c_\eta E_{hm(i)} \qquad (24)$$

where η_{sd} is a material parameter.

Yield deterioration is accounted for by introducing parameter v_s into the yield related smooth Heaviside function $_1$ defined in relation (13)

$$H_1 = v_s \left|\frac{\Phi\left(\{\sigma\}_{m(i)},\{\eta\}_{m(i)} s\right)}{\Phi_0}\right|^N, \quad N \geq 2 \qquad (25)$$

where in general v_s is a function of the hysteretic energy accumulated within the element

$$\dot{v_s} = \mathscr{K}_v\left(E_{hm(i)}\right) \qquad (26)$$

i	c_i	h_i
1	280e6 kPa	850
2	100e3 kPa	500
3	50e3 kPa	8
4	1e3 kPa	5
5	0.1 kPa	1

Table 1. Chaboche model parameters

A constant rate evolution law is also considered in this work, thus the variation of the strength deterioration parameter v_s is defined as

$$\left.\begin{array}{r} \dot{v_s} = c_s \\ v_s|_{E_h=0} = 1.0 \end{array}\right\} \Rightarrow v_s = 1.0 + c_s E_{hm(i)} \qquad (27)$$

where c_s is a user defined material parameter.

Example

To better demonstrate the influence of the hysteretic parameters implemented in the model the case of steel bar under uniaxial tension is considered. The elastic modulus of the bar is $E_s = 210 GPa$ and the initial yield stress $s_y = 235 MPa$. The following parameters are considered for the smooth model, namely $n = 2$ and $\beta = \gamma = 0.5$. A von-Mises yield criterion is considered. Two cases of hardening are examined. In the first, linear kinematic hardening is considered with the hardening modulus $H = 4 GPa$. The hardening function G in relation (18) is therefore defined as

$$G = 4\frac{\partial\Phi}{\partial\{\sigma\}}$$

In the second case, a Chaboche additive nonlinear kinematic hardening rule is considered (Chaboche 1991), where hardening function is defined as:

$$G = \frac{\partial\Phi}{\partial\sigma}\left(\sum_1^5 \frac{2}{3}h_i - \sqrt{\frac{2}{3}}c_i\eta\right) \qquad (28)$$

The model parameters for the Chaboche kinematic hardening are presented in Table 1.

The bar is subjected to sinusoidal imposed strain according to the following equation

$$\varepsilon = \frac{0.01}{\pi}sin(\pi t)$$

First, the analysis is performed considering no degradation effects, thus setting $c_\eta = c_s = 0$ in equations (24) and (27) respectively. The resulting stress-strain diagrams are presented in Fig. 2. Next, stiffness degradation and strength deterioration are taken into account by setting $c_\eta = 0.0000002$ and $c_s = 0.000001$ respectively. The corresponding results are presented in Fig. 3.

The hysteretic multiscale finite element method

Discrete formulation at the micro-scale

The discrete formulation is derived on the basis of the following rate form of the Principle of Virtual Work as in
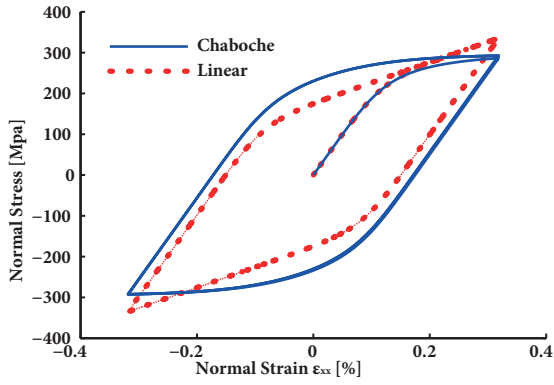
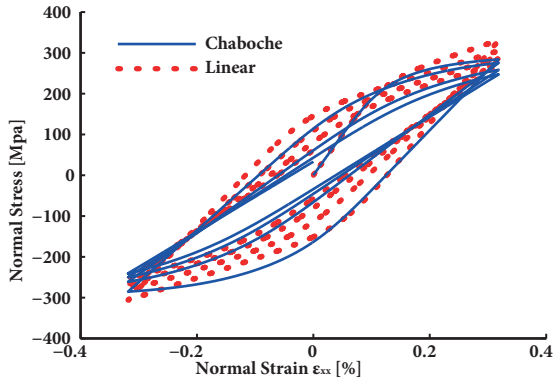**Figure 2.** Stress-strain diagrams - no degradations

Figure 3. Stress-strain diagrams - stiffness degradation/ strength deterioration

Washizu (1983)

$$\int_{V_e} \{\varepsilon\}_{m(i)}^T \{\dot\sigma\}_{m(i)} \, dV_e = \{d\}_{m(i)}^T \left\{\dot f\right\}_{m(i)} \quad (29)$$

where V_e is the volume of the discrete element, $\{d\}_{m(i)}$ is the vector of nodal displacements and $\left\{\dot f\right\}_{m(i)}$ is the vector of energy conjugate nodal forces. Substituting equation (9) into the variational principle (29) the following relation is derived:

$$\int_{V_e} \{\varepsilon\}_{m(i)}^T v_\eta [D]_{m(i)} \left(\{\dot\varepsilon\}_{m(i)} - \{\dot\varepsilon^{pl}\}_{m(i)} \right) dV_e = $$
$$= \{d\}_{m(i)}^T \left\{\dot f\right\}_{m(i)} \quad (30)$$

Performing some algebraic manipulations and also considering that $v_\eta \geq 1.0$ the following expression is derived:

$$\mathscr{I}_{el} - \mathscr{I}_{pl} = \frac{1}{v_\eta} \{d\}_{m(i)}^T \left\{\dot f\right\}_{m(i)} \quad (31)$$

where

$$\mathscr{I}_{el} = \int_{V_e} \{\varepsilon\}_{m(i)}^T [D]_{m(i)} \{\dot\varepsilon\}_{m(i)} dV_e \quad (32)$$

and

$$\mathscr{I}_{pl} = \int_{V_e} \{\varepsilon\}_{m(i)}^T [D]_{m(i)} \{\dot\varepsilon^{pl}\}_{m(i)} dV_e \quad (33)$$

In this work, the isoparametric interpolation scheme is considered for the displacement field

$$\{d\}_{m(i)} = [N] \{u\}_{m(i)} \quad (34)$$

where $[N]_{m(i)}$ is the shape function matrix. The corresponding strain-displacement relation is derived through compatibility (Zienkiewicz et al. 2005) and assumes the following form

$$\{\varepsilon\}_{m(i)} = [B] \{u\}_{m(i)} \quad (35)$$

where $[B]$ is the strain-interpolation matrix.

An additional interpolation scheme is introduced for the plastic deformation

$$\left\{\dot\varepsilon^{pl}\right\}_{m(i)} = [N]_e \left\{\dot\varepsilon_{cq}^{pl}\right\}_{m(i)} \quad (36)$$

where $\left\{\varepsilon_{cq}^{pl}\right\}_{m(i)}$ is the vector of stains measured at properly defined collocation points and $[N]_e$ is the corresponding interpolation matrix.

Substituting relations (35) and (36) onto equation (30), the following relation is derived

$$\left[k^{el}\right]_{m(i)} \left\{\dot d\right\}_{m(i)} - \left[k^h\right]_{m(i)} \left\{\dot\varepsilon_{cq}^{pl}\right\}_{m(i)} = \frac{1}{v_\eta} \left\{\dot f\right\}_{m(i)} \quad (37)$$

where

$$\left[k^{el}\right]_{m(i)} = \int_{V_e} [B]^T [D]_{m(i)} [B] \, dV_e \quad (38)$$

is the element elastic stiffness matrix while $\left[k^h\right]_{m(i)}$

$$\left[k^h\right]_{m(i)} = \int_{V_e} [B]^T [D]_{m(i)} [N]_e \, dV_e \quad (39)$$

is the hysteretic matrix. Both $\left[k^{el}\right]_{m(i)}$ and $\left[k^h\right]_{m(i)}$ are constant. Nonlinearity is introduced at the additional collocation points where plastic the evolution of plastic deformations is measured. This evolution can be generically defined in the form of equation (11).

In the case of the composite structure presented in Figure 1, the element elastic stiffness matrix $\left[k^{el}\right]_{m(i)}$ concides with the 24×24 stiffness matrix of the 8-node brick element (Cook et al. 2002). The size of the hysteretic matrix $\left[k^h\right]_{m(i)}$ depends also on the number of collocation points. Considering the case where full integration is performed and the collocation points are chosen to coincide with the Gauss point would result in a 24×48 hysteretic matrix.

Micro to Macro transformation

Considering zero initial conditions for brevity, rates in equation (38) are dropped and the following relation is established

$$\left[k^{el}\right]_{m(i)} \{d\}_{m(i)} - \left[k^h\right]_{m(i)} \left\{\varepsilon_{cq}^{pl}\right\}_{(i)} = \frac{1}{v_\eta} \{f\}_{m(i)} \quad (40)$$

Substituting equation (6) into equation (40) and premultiplying with $[N]_{m(i)}^T$ the following relation is derived:

$$\left[k^{el}\right]_{m(i)}^M \{d\}_M - \left[k^h\right]_{m(i)}^M \left\{\varepsilon_{cq}^{pl}\right\}_{(i)} = \frac{1}{v_\eta} \{f\}_{m(i)}^M \quad (41)$$

where

$$\left[k^{el}\right]_{m(i)}^{M} = [N]_{m(i)}^{T} \left[k^{el}\right]_{m(i)} [N]_{m(i)} \qquad (42)$$

is the elastic stiffness matrix of the i_{th} micro-element mapped onto the macro-element degrees of freedom while $\left[k^{h}\right]_{m(i)}^{M}$ is the hysteretic matrix of the i_{th} micro-element, evaluated by the following relation:

$$\left[k^{h}\right]_{m(i)}^{M} = [N]_{m(i)}^{T} \left[k^{h}\right]_{m(i)} \qquad (43)$$

Finally, $\{f\}_{m(i)}^{M}$ in equation (41) is the equivalent nodal force vector of the micro-element mapped onto the macro-nodes of the coarse element.

$$\{f\}_{m(i)}^{M} = \frac{1}{v_{\eta}} [N]_{m(i)}^{T} \{f\}_{m(i)} \qquad (44)$$

Equation (41) maps the micro-element equilibrium equation established in equation (40) from the micro-scale to the macro-scale. The micro-displacement components $\{u\}_{m(i)}$ are mapped onto their macro-counterparts through relation (6). Consequently, the elastic micro-constitutive behavior is communicated across scales through the EMsFEM numerical mapping. Inelasticity is accounted for in the micro-scale through the evolution of the micro-plastic deformation quantities $\left\{\varepsilon_{cq}^{pl}\right\}_{(i)}$ and mapped onto the macro-scale through the transformed hysteretic matrix $\left[k^{h}\right]_{m(i)}^{M}$.

Relations (42) and (43) are then assembled at the macro-scale to derive the coarse element equilibirum equation which assumes the following form

$$[K]_{CR(j)}^{M} \{d\}_{M} = \{f\}_{M} - \{f_{h}\}_{M} \qquad (45)$$

where $[K]_{CR(j)}^{M}$ is the equivalent stiffness matrix of the coarse element derived as

$$[K]_{CR(j)}^{M} = \sum_{1}^{i} \left[k^{el}\right]_{m(i)}^{M} \qquad (46)$$

while $\{f\}_{M}$ is the correspodning nodal force vector assembled from the contributions of the mapped micro-nodal force components defined in relation (44) and $\{f_{h}\}_{M}$ is the force vector of the plastic components evaluated as

$$\{f_{h}\}_{M} = \sum_{i=1}^{m_{el}} \left[k^{h}\right]_{m(i)}^{M} \left\{\varepsilon_{cq}^{pl}\right\}_{m(i)} \qquad (47)$$

Equation (45) is derived upon enforcing the energy equivalence principle between the deformation energy of the coarse element and the deformation energy of the corresponding micro-mesh (Triantafyllou and Chatzi 2014). This is not an assumption of the method a relation that holds as the coarse element is a mathematical entity whose mechanical properties are only defined at the micro-scale. Having defined the equivalent coarse element elastic stiffness and hysteretic matrice, the direct stiffness method is implemented to finally derive the governing equations at the structural level. Defining as $ndof_{M}$ the number of the free macro-degrees of freedom, the equations of motion of the structure assume the following form

$$[M] \left\{\ddot{U}\right\}_{M} + [C] \left\{\dot{U}\right\}_{M} + [K] \{U\}_{M} = \{P\}_{M} \qquad (48)$$

The coarse mesh $(ndof_{M} \times 1)$ nodal load vector $\{P\}_{M}$ in relation (48) is derived as

$$\{P\}_{M} = \{F\}_{M} + \{F_{h}\}_{M} \qquad (49)$$

where $\{F\}_{M}$ is the $(ndof_{M} \times 1)$ vector of externally applied loads and $\{F_{h}\}_{M}$ is the $(ndof_{M} \times 1)$ hysteretic load vector assembled for the whole structure. Matrices $[M]$, $[C]$ and $[K]$ are the $(ndof_{M} \times ndof_{M})$ mass, viscous damping and elastic stiffness matrix of the structure evaluated at the coarse mesh.

Equations (48) are supplemented by the evolution equations of the micro-plastic strain components defined at the collocation points within the micro-elements. These equations can be established in the following form:

$$\left\{\dot{E}_{cq}^{pl}\right\}_{m} = [H] \{\dot{\varepsilon}_{cq}\}_{m} \qquad (50)$$

where the vector

$$\left\{\dot{E}_{cq}^{pl}\right\}_{m} = \left\{ \left\{\dot{\varepsilon}_{cq}^{pl}\right\}_{m(1)} \quad \cdots \quad \left\{\dot{\varepsilon}_{cq}^{pl}\right\}_{m(m_{el})} \right\}^{T} \qquad (51)$$

holds the plastic strain components evaluated at the collocation points of its micro-element and

$$\left\{\dot{E}_{cq}\right\}_{m} = \left\{ \{\dot{\varepsilon}_{cq}\}_{m(1)} \quad \cdots \quad \{\dot{\varepsilon}_{cq}\}_{m(m_{el})} \right\}^{T} \qquad (52)$$

Matrix $[H]$ in relation (50) is a block diagonal matrix that assumes the following form

$$[H] = \begin{bmatrix} \mathscr{A}_{(1)} & & [0] \\ [0] & \ddots & \\ & & \mathscr{A}_{(m_{el})} \end{bmatrix} \qquad (53)$$

where $\mathscr{A}_{(1)} = H_{1m(1)} H_{2m(1)} [R]_{m(1)}$ and $\mathscr{A}_{(m_{el})} = H_{1m(m_{el})} H_{2m(m_{el})} [R]_{m(m_{el})}$

Equations (50) are independent and thus can be solved in the micro-element level resulting in an implicitly parallel scheme. Furthermore, relation (53) depends on the current micro-stress state within each micro-element. Thus, a procedure needs to be established that downscales the macro-displacements $\{U\}_{M}$.

Any type of numerical integration method can be implemented to solve the equations of motion of the hysteretic multiscale formulation (48). In this work, the HHT numerical integration algorithm is used in conjunction with a Newton-Raphson iterative scheme to treat nonlinearity. Equations (50) are treated at the micro-element level by means of the cutting-plane algorithm although more robust approaches such as the Radial Return mapping algorithm can also be implemented. The compuatational aspects of the methodology presented herein are described in detail in Triantafyllou and Chatzi (2014).

Computational Model Validation

As aforementioned, validation of computational models may be discussed in relation to two main directions, namely the numerical and experimental validation approach.

Numerical Validation

Within the scope of what is discussed herein, it is evident that as the complexity of the system increases, the formulation of exact models becomes a challenging task. In validating the efficacy of the assumptions and simplifications that need be adopted, the Monte Carlo method comprises a useful tool for reliability prediction. Unlike many other mathematical models, system complexity is not a hurdle for this approach, which can handle dynamic systems of an imprecise nature.

Reliability models entail processes of a probabilistic nature. These processes usually analyze the effects of the combination of two or more input random variables onto the probability distribution of certain output random variables. In approaching such a problem one could resort to either analytical methods or to Monte-Carlo simulation. In the analytical method, the probability distributions associated with the output are derived via analytical formulations involving the probability distributions associated with the input. Since such a straightforward formulation is difficult to obtain depending on the problem at hand, Monte Carlo simulation offers a valuable alternative. In Monte-Carlo simulation, a sample space of the input parameter is generated via use of a random number and knowledge of its probability distribution function (pdf). By repeating this process for a large number of input samples, a picture of the distribution of the output random variable is attained, which ultimately leads into statistical estimates of parameters of interest, e.g. mean and standard deviation of failure probability, or maximum inter-storey drift ratios. Through a variety of implementations, the Monte Carlo simulation has surfaced as a robust and widely applied method in determining the reliability of a structural component or system (Kiureghian 1996; Beck and Au 2002). A more detailed explanation of the Monte-Carlo simulation within the scope of structural reliability is given in Laumakis and Harlow (2002). Nonetheless, it should be noted that Direct Monte Carlo simulation (DMCS) can be computationally expensive, which is why hybrid or semi-analytical methods have been developed (Cardoso et al. 2008).

Due to its ease of implementation and flexibility in handling any type of problem, the Monte Carlo method is applied in the example cases presented herein for the purpose of computational model validation. In what is of interest in this work, the set of random input variables comprises not only the structural's system properties but also the precision of the numerical model itself. In the first application example presented in Section **Examples**, the sensitivity of the performance of a composite system is assessed with regard to both of these quantities, namely the stiffness and strength parameters of the separate constituents, as well as the use of solver (fine-mesh FEM versus HMsFEM).

Experimental Validation

The second and most critical means of model validation is via direct comparison of the model prediction to the actual system response, either this is pertinent to experimentally observed response or field testing of large-scale structural systems. On the basis of this, System Identification methods provide a valuable toolkit for updating uncertain models of structural systems based on direct information from the system itself. The recent technological advances further enable the extraction of information from structures via production of low-cost sensor arrays that can be easily deployed on either a short- or long-term basis and based on which structural feedback is attained in various forms such as acceleration, velocity, displacement, or strain measurements.

The rich amount of data gathered from structural response can be used in an inverse problem setting for identifying structural characteristics that are not precisely known a-priori and for updating or even selecting appropriate simulation models. The second application presented in Section **Examples** discusses such an inverse problem formulation, where the goal is to infer the characteristic properties of the constituents, i.e., stiffness and strength, based on limited information of vibrational response in the form of acceleration measurements. The measurements are obtained via simulation of a testing process for the composite aluminum panel that is here used as an example test case.

The identification algorithm that is here utilized for joint state and parameter estimation is the Unscented Kalman Filter (UKF), which has been extensively utilized in previous works of the authors (Chatzis et al. 2014; Chatzi and Smyth 2009; Chatzi et al. 2010) and essentially constitutes an approximation of the standard Kalman Filter applicable for problems of joint state and parameter estimation. The UKF is a Bayesian approximation which succeeds in simulating non-linear behavior by approximating the state as a Gaussian random variable (GRV), represented by a set of carefully chosen deterministic points known as the Sigma Points. The interested reader is referred to the works of Julier and Uhlmann (1997), and Wan and van der Merwe (2000) for the implementation details.

In the joint state and parameter identification regime, the filter's structure is of the following form:

$$\left\{ \begin{array}{c} \mathbf{x}_{k+1} \\ \boldsymbol{\theta}_{k+1} \end{array} \right\} = \left\{ \begin{array}{c} F(\mathbf{x}_k, \boldsymbol{\theta}_k) \\ \boldsymbol{\theta}_k \end{array} \right\} + \mathbf{w}_k$$
$$\mathbf{y}_k = H(\mathbf{x}_k, \boldsymbol{\theta}_k) + \mathbf{v}_k \tag{54}$$

where $\mathbf{x}_k$ is the state variable vector comprising the displacements and velocities of a structural system undergoing dynamic loading, $\boldsymbol{\theta}_k$ are the time invariant parameters that are considered to be unknown or uncertain, $\mathbf{w}_k$ is a zero mean Gaussian process noise vector with covariance matrix $\mathbf{Q}_k$, $\mathbf{y}_k$ is the observation vector and $\mathbf{v}_k$ is the zero mean Gaussian measurement noise vector with corresponding covariance matrix $\mathbf{R}_k$.

The process noise reveals the confidence placed into the accuracy of the system representation, i.e., the model of the system. The observation noise on the other hand reveals the confidence placed in the acquired measurement. The tuning of these quantities is critical depending on the task at hand. Additionally, functions F, H represent the system and observation model respectively. The flexibility of the UKF lies in the ability to incorporate loosely defined functions. In the implementation presented herein the developed HMsFEM framework is utilized as the model simulating the system response (function F), whereas a fine-mesh FEM is utilized for extraction of the measurement quantities, $\mathbf{y}_k$. The latter correspond to acceleration time histories at certain nodes of the structure. As this process
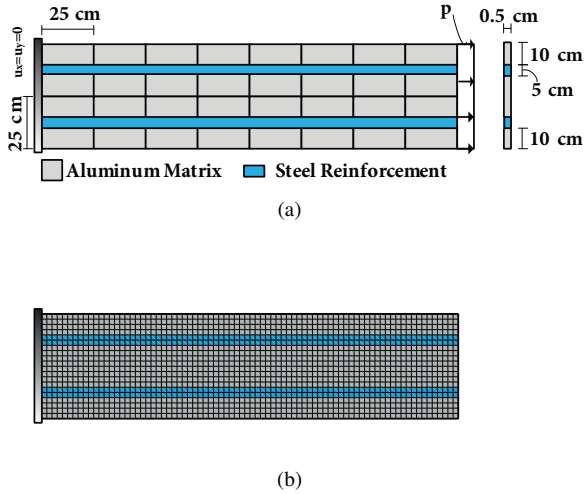
(a)

(b)

Figure 4. (a) Model Definition (b) Finite Element mesh

Figure 5. Force Displacement Loops (Mean Values)

is also a stochastic one involving numerous parallel forward simulation, for each discrete sigma point, the ability to use a reduced order model of the system which however provides sufficient accuracy is of the essence.

As discussed in the next Section the HMsFEM approach furnishes an invaluable tool for accurate yet accelerated computation, especially suited for problems of structural reliability or inverse formulations, that are concomitant to structural model validation.

Examples

Aluminum Panel - Non-degrading material

In this example, a sensitivity and reliability analysis pertaining to the dynamic response of a heterogeneous structure, with uncertain material properties, is performed. A fine meshed Finite Element model is considered as the detailed reference simulation and is cross-compared to a reduced order forward model developed via the HMsFE method. For the purpose of this parametric analysis the case of an aluminum sheet is considered, reinforced with two steel strips (Fig. 4(a)). The length, width and height of the beam are $L_m = 200cm$, $b_m = 0.5cm$ and $h_m = 50cm$ respectively. The height of the steel strips is $h_f = 5cm$. The constituents are assumed to be elastic-perfectly plastic with deterministic Poisson ratios $\nu_a = 0.33$ and $\nu_s = 0.3$ for the aluminum and steel respectively. The elastic moduli and the corresponding yield stresses of the materials are considered to be random variables. The Log-Normal distribution is used for all random variables with corresponding mean values $E_{ma} = 70GPa$ and $f_{ya} = 214MPa$ for the aluminum and $E_{ms} = 200GPa$ and $f_{ys} = 235MPa$ for the steel. A varying amplitude sinusoidal deterministic pressure load is considered at the free end defined as $p(t) = 20000t sin(\pi t)kPa$.

The fine meshed finite element model presented in Fig. 4(b) consists of 1600 linear quadrilateral plane stress elements with a total of 3358 free degrees of freedom. The multiscale finite element model is formulated by 16 plane stress coarse elements. The corresponding
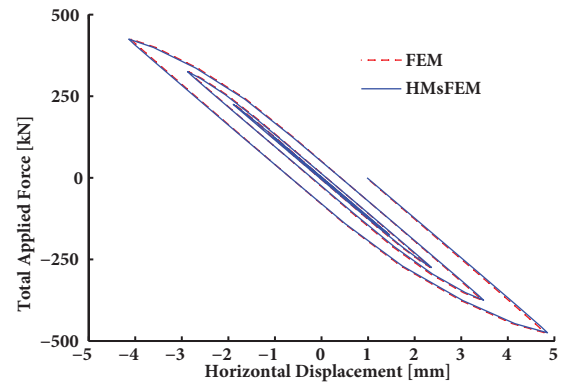
representative RVE consists of 100 plane stress elements. The periodic boundary condition assumption is used to evaluate the micro-basis interpolation functions. In Figure 5, the force-displacement hysteretic loops derived from the two formulations for the mean values of the random variables are presented. The differences between the two formulations are marginal.

Next, a total 5000 Monte Carlo iterations is performed in each model, considering a Latin Hypercube sampling scheme. Different random seeds and therefore different sets of random variables are used for the FEM and HMsFEM case, with the purpose of obtaining an unbiased comparison. The derived data sets of the effective elastic stiffness evaluated from the response of the FEM and HMsFEM analysis cases are presented in Fig 6(a) and 6(b) respectively. This effective value is calculated as the slope of the elastic region of the force-displacement diagram for the first cycle of loading. Furthermore, the histograms of the maximum displacements are presented in Fig. 7, providing in this way a measures that quantifies structural response under loads that push the system into the plastic region, thereby serving as a tool for assessing structural reliability. The statistical properties of the two data sets are in very good agreement.

In Fig. 8(a) the derived PDFs of the macroscopic elastic horizontal stiffness of the two models is presented. The derived PDFs are found to fit a generalized extreme value distribution function of the II type. The results obtained from the HMsFE model are almost identical to the results obtained from the fine meshed FEM model. In Fig. 8(b) the derived probability density functions of the maximum axial displacement are presented. The corresponding statistical data is found to fit the extreme value distribution function. The results obtained from the two different models are in good agreement, with the relative difference in the statistical parameters of the parametric PDEs being less than 0.5%.

Aluminum Panel - Degrading material

In this case, the variability of the strength deterioration and stiffness degradation parameters is also considered. To better illustrate their effect on the dynamic response of the structure, the following, constant amplitude, sinusoidal excitation is considered in this case
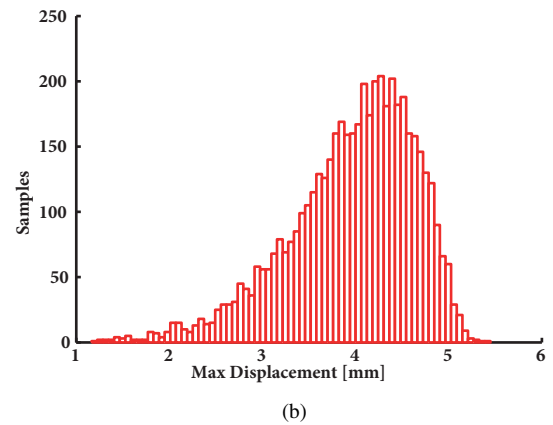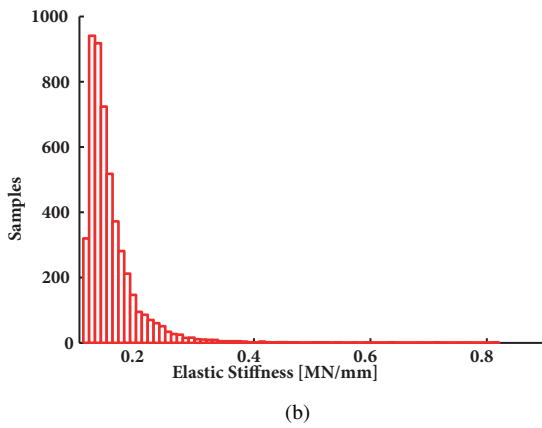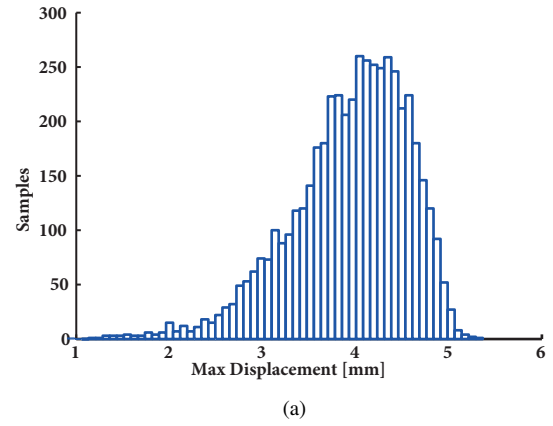
$$p(t) = 250000 sin(\pi t)kPa$$

(a)

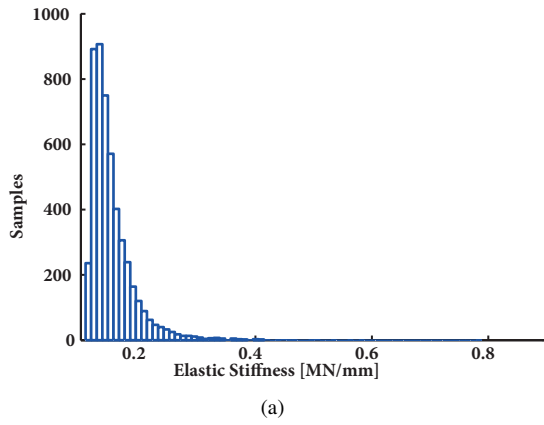

(b)

Figure 6. Elastic Stiffness Histogram (a) FEM (b) HMsFEM

Variable	Min	Max
E_{ma}	62500000 kPa	67500000 kPa
f_{ya}	200000 kPa	242000 kPa
$c_{\eta m}$	2.5e-7	2.5e-6
c_{sm}	5.0e-7	5.0e-6
E_s	200000000 kPa	231000000 kPa
f_{ys}	225000 kPa	247500 kPa
$c_{\eta s}$	2.5e-7	2.5e-6
c_{ss}	5.0e-7	5.0e-6

Table 2. Random Variable limit values

The random variables in this case are the elastic moduli, yield stress and the stiffness degradation and strength deterioration parameters of the constituents. The uniform distribution is considered for all variables and the limit values considered are presented in Table 2.

In Fig. 9, the total applied force versus the center-point axial displacement at the tip of the cantilever is presented. The results obtained from the two procedures are practically identical. In this case, the analysis conducted using the HMsFEM procedure concluded in 900 sec while the corresponding analysis time using the standard FEM procedure was 4626 sec, amounting to a significant reduction in the computational toll involved.

In this case 2000 Monte Carlo simulations were performed for each one of the solution approaches. Contrary to the case examined in Section **Aluminum Panel - Non-degrading material** the same pool of random variables is considered for

(a)

(b)

Figure 7. Maximum Displacement Histogram (a) FEM (b) HMsFEM

both cases. The derived results are again compared in terms of the estimated PDFs of the response variables.

In Fig. 10(a) and 10(b) the histograms of the derived maximum displacements are presented for the case of the HMsFEM and FEM analysis respectively. The HMsFEM approach results in a slightly stiffer configuration as compared to the FE method. The same trend is also revealed form the histograms of the residual displacement presented in Fig. 11(a) and 11(b) for the multiscale and finite element methods respectively.

In Fig. 12(a), the estimated PDFs for the maximum displacement are compared while in Fig. 12(b) the derived PDFs for the residual displacement (due to plastic deformation) are presented.

Inverse Problem Formulation

In this example, a structure similar to the previous composite panel is revisited, under the prism of parameter identification. The aluminum sheet of Figure 4(a) is once again considered with a length, width and height of $L_m = 200cm$, $b_m = 0.3cm$ and $h_m = 50cm$ respectively. The height of the steel strips is $h_f = 5cm$. A concentrated mass of $15tn$ is attached on the free end of the beam. A random pressure load is considered at the free end defined as $p(t)$ $NID(0, \sigma_e^2)$ with NID denoting a Normally Independently Distributed process with the indicated mean and variance. This type of load, illustrated in Figure 14,
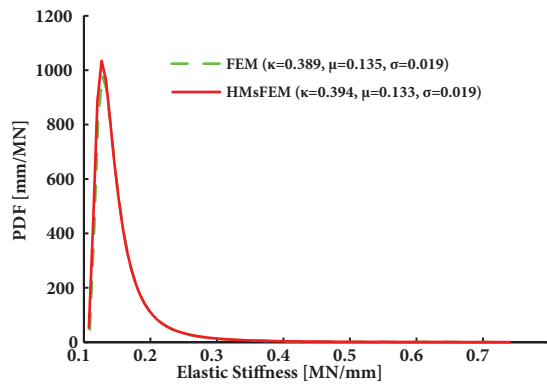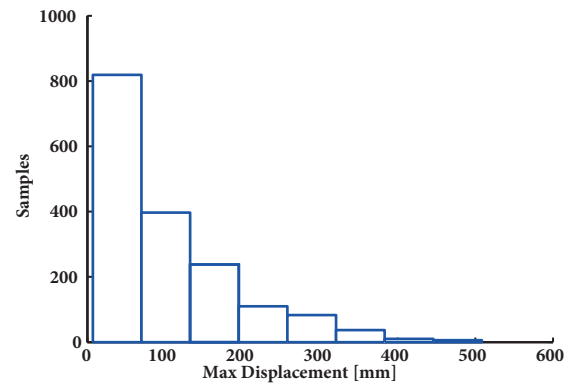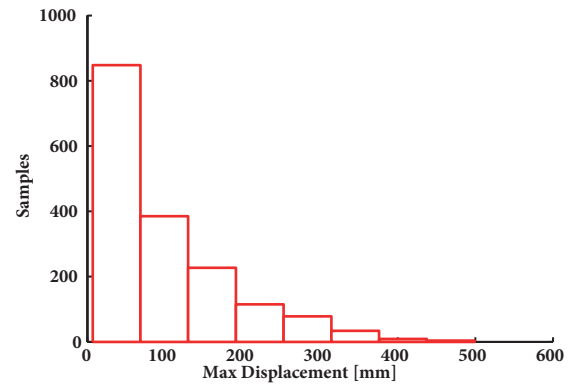
(a)
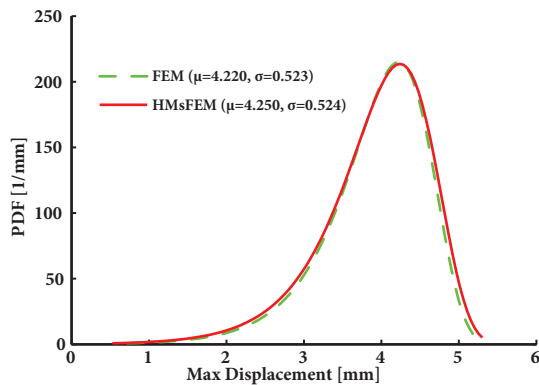
(b)

Figure 8. (a) Elastic Stiffness PDFs (b) Maximum Displacement PDFs

(a)

(b)

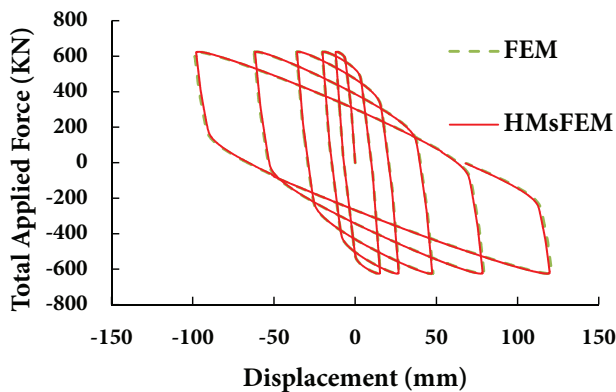**Figure 10.** Maximum Displacement Histogram (a) FEM (b) HMsFEM

Figure 9. Degrading Material: Force Displacement Loops (Mean Values)

allows for the simulation of a simple testing procedure driven either via random excitation or possibly a suitable shaking device with an appropriate stinger, exerting an axial load on the lumped $15tn$ mass.

The goal is to utilize information from the structure in the form of acceleration measurements obtained at a finite set of sensor locations, nine in total, as indicated in Figure 13, in order to identify the properties of the constituents involved. The four constitutive parameters, namely the elastic stiffness and yield stress of each of the two constituents, are considered as unknown a-priori or,

more precisely, as uncertain. An off initial assumption is made on the values of these parameters, which is utilized as the initial condition to be fed into the UKF algorithm. The corresponding initial values are $\boldsymbol{\theta}_1^0 = E_{ma} = 87.5GPa$ and $\boldsymbol{\theta}_2^0 = f_{ya} = 267.5MPa$ for the aluminum and $\boldsymbol{\theta}_3^0 = E_{ms} = 241.5GPa$ and $\boldsymbol{\theta}_4^0 = f_{ys} = 211.5MPa$ for the steel. The true parameter values are on the other hand set as $\boldsymbol{\theta}_1 = E_{ma} = 70GPa$ and $\boldsymbol{\theta}_2 = f_{ya} = 210MPa$ for aluminum and $\boldsymbol{\theta}_3 = E_{ms} = 210GPa$ and $\boldsymbol{\theta}_4 = f_{ys} = 235MPa$ for steel.

A reference forward analysis is performed in ABAQUS, employing a fine mesh; this serves as the "actual" response, utilized here as the equivalent of an experimental testing process. Therefore, the measurement vector $\mathbf{y_k}$, comprising nine acceleration data sets, to be fed into equation (54) of the UKF, is herein generated via an independent numerical simulation. The crucial component lies in the utilization of the forward (or process) model for the UKF. As explained earlier, the UKF is formulated using a discrete set of samples, termed the Sigma Points. The number of these Sigma Points equals $2 * L + 1$, where L is the size of the augmented state of the system. For a joint state-parameter identification problem, this augmented vector comprises the system's displacements and velocities at all degrees of freedom, as well as the unknown parameters (four in this example). It therefore becomes evident, that if one is to utilize a finely meshed model construed in ABAQUS, the dimension of the system would be too large for numerical computation. Even more importantly due to memory limitations, there
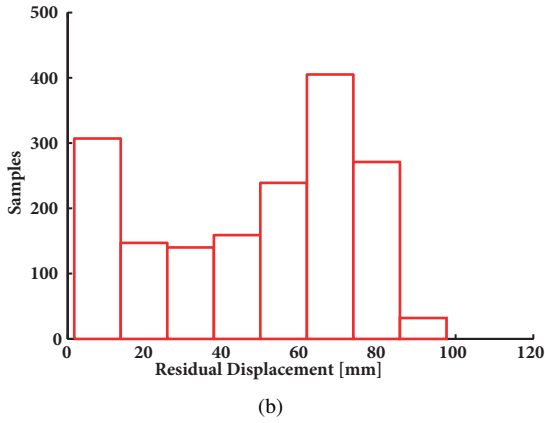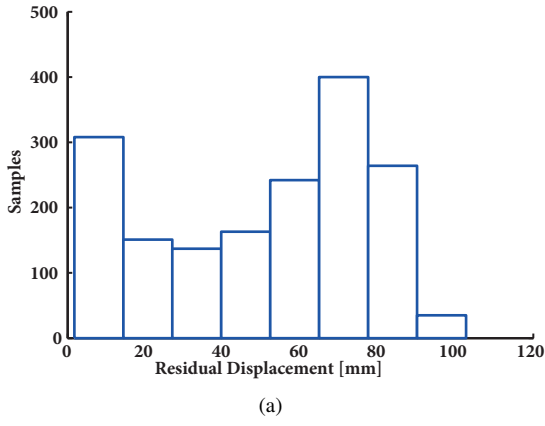
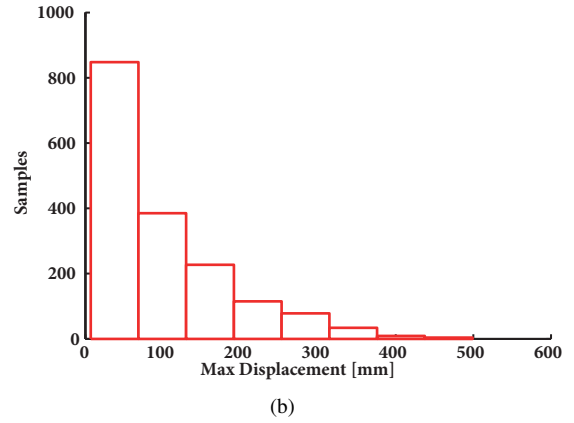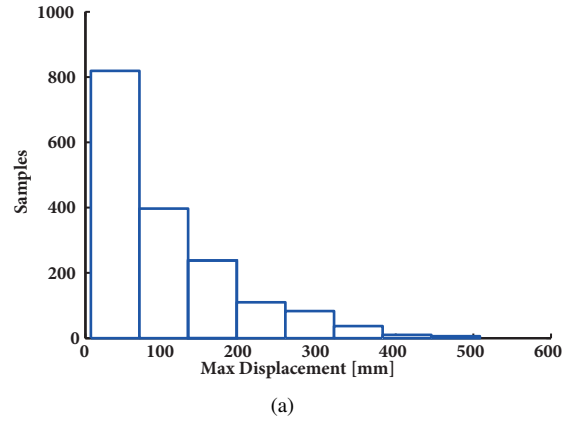**Figure 11.** Residual Displacement Histogram (a) FEM (b) HMsFEM

Figure 12. (a) Maximum Displacements PDFs (b) Residual Displacement PDFs

exists a critical matrix size, and therefore an associated mesh refinement, for which calculations would be prohibited. A means for solving this problem is delivered through the utilization of the proposed HMsFEM approach. In what follows, the process and observation functions denoted as F, H in (54) are replaced via the HMSFEM solver between successive time steps. A coarse mesh of 24 nodes is utilized, bringing the state dimension down to a dimension $L = 2 * 24 + 4 = 52$. The corresponding Sigma Point set therefore comprises a total of $2L + 1 = 109$ components. Furthermore, the Sigma Point runs are in fact independent, allowing for the parallel execution of these forward runs. The identification process is consequently initiated with the following settings for the filter. An initial covariance of the state, $\mathbf{P_x}$, of the order of $1e - 13$ is assigned. The process and observation noise covariance matrices, $\mathbf{Q}_k$ and $\mathbf{R}_k$ respectively, are set as a diagonal with diagonal components equal to $1e - 13$ and $1e - 5$ correspondingly. For facilitating the filter implementation, and avoiding numerical errors, the parameter values are normalized with a target values set at 0.01 for all four constitutive parameters.

The results of the identification process are summarized in Figures 15-18. Figures 15-16 summarize the velocity predictions of the filter for both an observed (node #3), i.e., monitored via a sensor, as well as an unobserved (node #21) degree of freedom. It is noted that in both cases, the filter furnishes a very accurate estimation of the corresponding nodal velocities. An integration error, relating as well to the selected levels of process noise, is however noticeable in
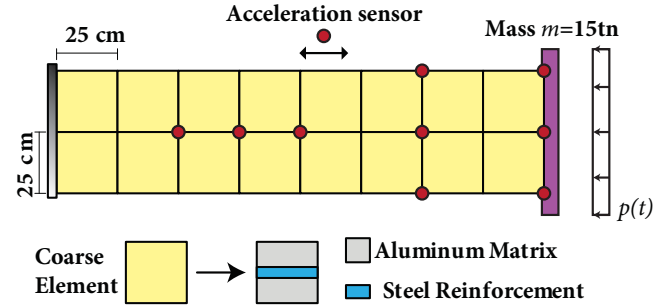

Figure 13. Acceleration sensor locations

the displacement estimates. This accumulation of integration errors resulting in displacement drifts is not uncommon as noted in Chatzi and Fuggini (in press), nonetheless this does not create a hindrance in the particular inverse problem solution.

The primary target of this inverse formulation is the extraction of the true parameters that characterize the structural properties, i.e., the stiffness and strength characteristics. Figure 19 indicates the convergence of the algorithm to the true, "normalized" parameter value which is set to 0.01 (unitless) for all parameters. The successful utilization of the filter is enabled through the implementation of the multiscale scheme. For the purposes of comparison, it is mentioned than on a PC fitted with an Intel i7 processor and 32 GB of RAM. utilizing all 4 cores, the time allocated for the analysis was approximatelly 4 hrs,
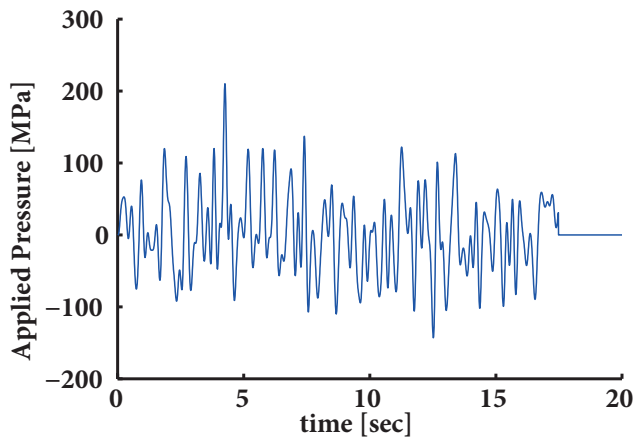
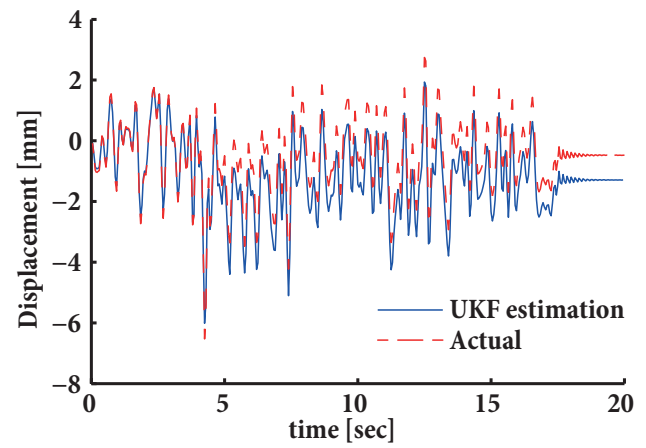**Figure 14.** Time history plot of the randomly generated input load.

Figure 15. Observed Node 3 velocity time-history estimate (blue) versus actual value (red).
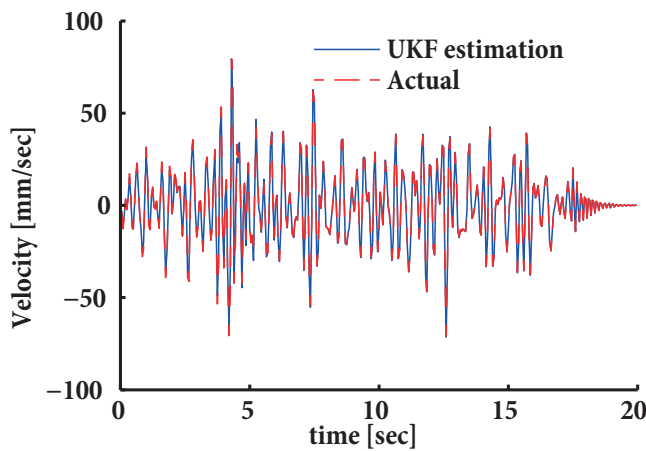

Figure 16. Unobserved Node 21 velocity time-history estimate (blue) versus actual value (red).
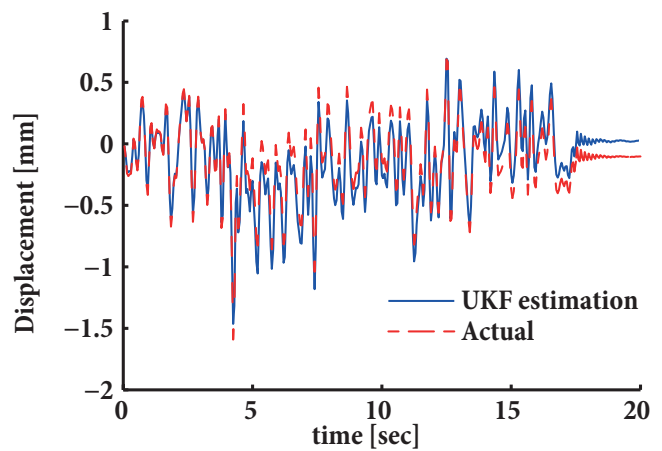

Figure 17. Observed Node 3 displacement time-history estimate (blue) versus actual value (red).

Figure 18. Unobserved Node 21 displacement time-history estimate (blue) versus actual value (red).
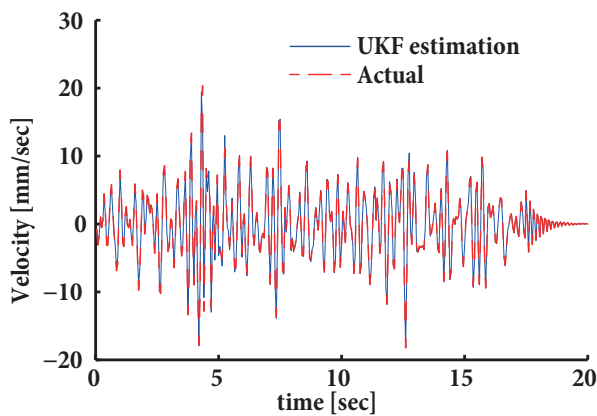
case of nonlinear hysteretic response, where the cost of computation forms a major concern.
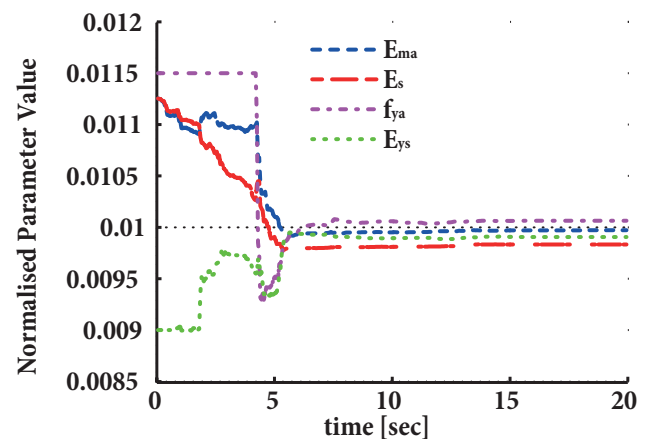
Figure 19. Constitutive parameters estimates versus the reference (normalized) value (black line).

whereas if the ABAQUS model were to be employed using the Finite Element mesh presented in Figure 4(b), a prohibitive total time of 4 days would be delivered. It is therefore pointed out, that the appropriate combination of advanced modeling tools with appropriate identification and uncertainty quantification techniques can enable the validation of computational mechanics models seeking to accurately reproduce structural response, especially in the

Conclusions

In this work, a numerical procedure for the computationally efficient simulation of nonlinear hysteretic response of multi-phase systems is presented, within the context of model validation. The proposed methodology termed the Hysteretic Multiscale Finite Element Method (HMsFEM) is formulated within the framework of the Enhanced Multiscale Finite Element method (MsFEM), where the fine-scale is modeled using a hysteretic finite element approach. Using this method, inelasticity is treated at the micro-level, introducing additional hysteretic degrees of freedom that evolve according to a generic multiaxial smooth hysteretic law. The developed modeling approach is utilized for the purposes of model validation; firstly, in the context of reliability analysis through cross-assessment against a fine-mesh model developed in an independent analysis program (ABAQUS); and secondly, for an inverse problem where the identification of constitutive parameters via availability of acceleration response data is sought. The derived results demonstrate the potential of utilizing the proposed approach as a computationally accelerated yet sufficiently accurate surrogate model in problems of nonlinear dynamic analysis of heterogeneous structures; a problem which by default comprises a computationally challenging task. The proposed approach provides a means of assessing model credibility as well as testing the validity of adopted assumptions concerning not only the model structure, but additionally the characteristic properties of associated models.

Acknowledgements

References

Aboudi J (2013) *Micromechanics of Composite Materials*. Butterworth-Heinemann, Oxford.

Abrosimov N and Kulikova N (2011) Parameter identification in viscoelastic strain models for composite materials by analyzing impulsive loading of shells of revolution. *Mechanics of Solids* 46(3): 368–379. DOI:10.3103/S0025654411030046.

Armenakas AE (2006) *Advanced Mechanics of Materials and Applied Elasticity*. CRC Press, Taylor and Francis Group, New York.

Babuška I (1975) Homogenization approach in engineering. Technical Report ORO–3443-58; TN-BN–828 United States; NSA-33-022692.

Bažant ZP and Daniel IM (1996) Size effect and fracture characteristics of composite laminates. *Journal of Engineering Materials and Technology* 118(3): 317–324.

Beck J and Au S (2002) Bayesian updating of structural models and reliability using Markov Chain Monte Carlo simulation. *Journal of Engineering Mechanics* 128(4): 380–391. DOI: 10.1061/(ASCE)0733-9399(2002)128:4(380).

Belingardi G, Beyene AT and Koricho EG (2013) Geometrical optimization of bumper beam profile made of pultruded composite by numerical simulation. *Composite Structures* 102(0): 217 – 225.

Burguete RL, Lampeas G, Mottershead JE, Patterson EA, Pipino A, Siebert T and Wang W (2013) Analysis of displacement fields from a high-speed impact using shape descriptors. *The Journal of Strain Analysis for Engineering Design* DOI:10. 1177/0309324713498074.

Cardoso JB, de Almeida JR, Dias JM and Coelho PG (2008) Structural reliability analysis using monte carlo simulation and neural networks. *Advances in Engineering Software* 39(6): 505 – 513. DOI:http://dx.doi.org/10.1016/j.advengsoft.2007. 03.015.

Chaboche J (1991) On some modifications of kinematic hardening to improve the description of ratchetting effects. *International Journal of Plasticity* 7(7): 661–678.

Chatzi E and Fuggini C (in press) Online correction of drift in structural identification using artificial white noise observations and an unscented kalman filter. *Smart Structures and Systems, Special Volume on Errors / uncertainties in sensors for Structural Health Monitoring* .

Chatzi EN and Smyth AW (2009) The unscented Kalman filter and particle filter methods for nonlinear structural system identification with non-collocated heterogeneous sensing. *Structural Control and Health Monitoring* 16(1): 99–123. DOI: 10.1002/stc.290.

Chatzi EN, Smyth AW and Masri SF (2010) Experimental application of on-line parametric identification for nonlinear hysteretic systems with model uncertainty. *Structural Safety* 32(5): 326–337.

Chatzis M, Chatzi E and Smyth A (2014) An experimental validation of time domain system identification methods with fusion of heterogeneous data. *Earthquake Engineering & Structural Dynamics* : n/a–n/aDOI:10.1002/eqe.2528.

Clément A, Soize C and Yvonnet J (2013) Uncertainty quantification in computational stochastic multiscale analysis of nonlinear elastic materials. *Computer Methods in Applied Mechanics and Engineering* 254(0): 61 – 82. DOI:http://dx. doi.org/10.1016/j.cma.2012.10.016.

Cook RD, Malkus DS, Plesha ME and Witt RJ (2002) *Concepts and applications of finite element analysis*. John Wiley & Sons, Inc., New York.

Efendiev Y, Ginting V, Hou T and Ewing R (2005) Accurate multiscale finite element methods for two-phase flow simulations. *J. Comput. Phys* .

Efendiev Y and Hou TY (2009) *Multiscale Finite Element Methods, Surveys and Tutorials in the Applied Mathematical Sciences*, volume 4. Springer.

Ekel'chik V (2007) Resonance methods for determining the complex shear moduli of orthotropic composites. *Mechanics of Composite Materials* 43(6): 487–502. DOI:10.1007/ s11029-007-0046-7.

Erlicher S (2003) *Hysteretic degrading models for the low-cycle fatigue behaviour of structural elements: theory, numerical aspects and applications*. PhD Thesis, Department of Mechanical and Structural Engineering, University of Trento, Italy.

Erlicher S and Point N (2004) Thermodynamic admissibility of bouc-wen type hysteresis models. *Comptes Rendus Mcanique* 332(1): 51 – 57. DOI:http://dx.doi.org/10.1016/j.crme.2003. 10.009.

Felipe-Sesé L, Siegmann P, Díaz FA and Patterson EA (2014) Simultaneous in-and-out-of-plane displacement measurements using fringe projection and digital image correlation. *Optics and Lasers in Engineering* 52(0): 66 – 74. DOI:http://dx.doi.org/10.1016/j.optlaseng.2013.07.025.

Frederiksen P (1997) Experimental procedure and results for the identification of elastic constants of thick orthotropic plates. *Journal of Composite Materials* 31: 360–382.

Geers MGD, Kouznetsova VG and Brekelmans WAM (2010) Multi-scale computational homogenization: Trends and challenges. *Journal of Computational and Applied Mathematics* 234(7): 2175–2182.

Hansun TT (2009) Homogenization of dynamic laminates. *Journal of Mathematical Analysis and Applications* 354(2): 518 – 538. DOI:http://dx.doi.org/10.1016/j.jmaa.2008.12.058.

He X and Ren L (2005) Finite volume multiscale finite element method for solving the groundwater flow problems in heterogeneous porous media. *Water Resources Research* 41(10): 1–15.

Iwan WD (1967) On a class of models for the yielding behavior of continuous and composite systems. *Journal of Applied Mechanics* 34(3): 612–617.

Julier SJ and Uhlmann JK (1997) A New Extension of the Kalman Filter to Nonlinear Systems. In: *Proc. of AeroSense: The 11th Int. Symp. on Aerospace/Defense Sensing, Simulation and Controls*.

Kanouté P, Boso DP, Chaboche JL and Schrefler BA (2009) Multiscale methods for composites: A review. *Archives of Computational Methods in Engineering* 16(1): 31–75.

Kiureghian AD (1996) Structural reliability methods for seismic safety assessment: A review. *Engineering Structures* 18(6): 412 – 424. DOI:http://dx.doi.org/10.1016/0141-0296(95)00005-4.

Laumakis PJ and Harlow G (2002) Structural reliability and Monte Carlo simulation. *International Journal of Mathematical Education in Science and Technology* 33(3): 377–387. DOI:10.1080/00207390210125729.

Liu D, Raju BB and Dang X (1998) Size effects on impact response of composite laminates. *International Journal of Impact Engineering* 21(10): 837 – 854.

Lubliner J (2008) *Plasticity Theory*. New York: Dover Publications.

Maletta C and Pagnotta L (2004) On the determination of mechanical properties of composite laminates using genetic algorithms. *International Journal of Mechanics and Materials in Design* 1(2): 199–211. DOI:10.1007/s10999-004-1731-5.

Maury B (2008) Numerical analysis of a finite element/volume penalty method. In: Glowinski R and Neittaanmki P (eds.) *Partial Differential Equations*, *Computational Methods in Applied Sciences*, volume 16. Springer Netherlands. ISBN 978-1-4020-8757-8, pp. 167–185. DOI:10.1007/978-1-4020-8758-5_9. URL http://dx.doi.org/10.1007/978-1-4020-8758-5_9.

Munch E, Launey ME, Alsem DH, Saiz E, Tomsia AP and Ritchie RO (2008) Tough, bio-inspired hybrid materials. *Science* 322(5907): 1516–1520.

Nemat-Naser S (1982) On finite deformation elasto-plasticity. *International Journal of Solids and Structures* 18(10): 857–872.

Nguyen VP, Stroeven M and Sluys LJ (2012) An enhanced continuousdiscontinuous multiscale method for modeling mode-i cohesive failure in random heterogeneous quasi-brittle materials. *Engineering Fracture Mechanics* 79(0): 78 – 102.

Pahlavanpour M, Moussaddy H, Ghossein E, Hubert P and Lvesque M (2013) Prediction of elastic properties in polymerclay nanocomposites: Analytical homogenization methods and 3d finite element modeling. *Computational Materials Science* 79(0): 206 – 215. DOI:http://dx.doi.org/10.1016/j.commatsci.2013.06.029.

Patterson EA, Feligiotti M and Hack E (2012) On the integration of validation, quality assurance and non-destructive evaluation. *The Journal of Strain Analysis for Engineering Design* DOI:10.1177/0309324712444681.

Peng X, Fan M, Hartley J and Al-Zubaidy M (2011) Properties of natural fibre composites made by pultrusion process. *Journal of Composite Materials* .

Pickett A (2002) Review of finite element simulation methods applied to manufacturing and failure prediction in composites structures. *Applied Composite Materials* 9(1): 43–58. DOI:10.1023/A:1012667427575.

Rikards R, Chate A, Steinchen W, Kessler A and Bledzki A (1999) Method for identification of elastic properties of laminates based on experiment design. *Composites Part B: Engineering* 30(3): 279 – 289. DOI:http://dx.doi.org/10.1016/S1359-8368(98)00059-6.

Rohatgi P (1994) Low-cost, fly-ash-containing aluminum-matrix composites. *JOM* 46(11): 55–59.

Saheb DN and Jog JP (1999) Natural fiber polymer composites: A review. *Advances in Polymer Technology* 18(4): 351–363.

Shang S and Yun GJ (2013) Stochastic finite element with material uncertainties: Implementation in a general purpose simulation program. *Finite Elements in Analysis and Design* 64(0): 65 – 78. DOI:http://dx.doi.org/10.1016/j.finel.2012.10.001.

Soares C, de Freitas M, Arajo A and Pedersen P (1993) Identification of material properties of composite plate specimens. *Composite Structures* 25(14): 277 – 285. DOI:http://dx.doi.org/10.1016/0263-8223(93)90174-O.

Strong AB (2008) *Fundamentals of Composites Manufacturing, Methods and Applications*. 2 edition. MI: Society of Manufacturing Engineers, Dearborn.

Tootkaboni M and Graham-Brady L (2010) A multi-scale spectral stochastic method for homogenization of multi-phase periodic composites with random material properties. *International Journal for Numerical Methods in Engineering* 83(1): 59–90. DOI:10.1002/nme.2829.

Triantafyllou S and Chatzi E (2014) A hysteretic multiscale formulation for nonlinear dynamic analysis of composite materials. *Computational Mechanics* 54(3): 763–787. DOI:10.1007/s00466-014-1032-2.

Triantafyllou S and Koumousis V (2014) Hysteretic finite elements for the nonlinear static and dynamic analysis of structures. *Journal of Engineering Mechanics* 140(6): 04014025–1–04014025–17. DOI:10.1061/(ASCE)EM.1943-7889.0000699.

Tucker CLI and Erwin L (1999) Stiffness predictions for unidirectional short-fiber composites: Review and evaluation. *Composites Science and Technology* 59(5): 655 – 671. DOI:http://dx.doi.org/10.1016/S0266-3538(98)00120-1.

Visintin A (1994) Differential models of hysteresis. In: *Applied Mathematical Sciences*, volume 111. Springer,.

Wan EA and van der Merwe R (2000) The Unscented Kalman Filter for Nonlinear Estimation. *Adaptive Systems for Signal Processing, Communications, and Control Symposium 2000* :

153–158.

Washizu K (1983) *Variational Methods in Elasticity and Plasticity*. Pergamon Press, Oxford.

Xu XF, Hu K, Beyerlein IJ and Deodatis G (2011) Statistical strength of hierarchical carbon nanotube composites. *International Journal for Uncertainty Quantification* 1(4): 279–295.

Yu Q and Fish J (2002) Multiscale asymptotic homogenization for multiphysics problems with multiple spatial and temporal scales: A coupled thermo-viscoelastic example problem. *International Journal of Solids and Structures* 39(26): 6429–6452.

Zhang HW, Wu JK and Lv J (2012) A new multiscale computational method for elasto-plastic analysis of heterogeneous materials. *Computational Mechanics* 49(2): 149–169.

Zienkiewicz OC, Taylor RL and Zhu J (2005) *The Finite Element Method: Its Basis and Fundamentals*. 6 edition. Elsevier, Amsterdam.